Date July 2007
Author P. de Jong, F. van Walree, J.A. Keuning, R.H.M. Huijsmans
Address Delft University of Technology
Ship Hydromechanics Laboratory
Mekelweg 2, 26282 CD Delft

TUDelft

Delft University of Technology

Evaluation of the Free Surface Evaluation in a Time-Domain Panel Method for the Seakeeping of High Speed Ships

by

Pepijn de Jong, Frans van Walree, Alexander Keuning and René Huijsmans

Report No. 1529-P **2007**

Proceedings of the 7th International Offshore and Polar Engineering Conference, Lisbon, Portugal, July 1-6, 2007, ISBN: 978-1-880653-68-0

Proceedings of the Seventeenth (2007) International Offshore and Polar Engineering Conference
Lisbon, Portugal, July 1-6, 2007

ISBN 978-1-880653-68-5; ISBN 1-880653-68-0(Set); ISSN 1098-6189 (Set)

Evaluation of the Free Surface Elevation in a Time-Domain Panel Method for the Seakeeping of High Speed Ships

Pepijn de Jong[†], *Frans van Walree*[‡], *Alexander Keuning*[†], *René H.M. Huijsmans*[†]
[†] Ship Hydromechanics and Structures, Delft University of Technology,
Delft, The Netherlands
[‡] Marin, Wageningen, The Netherlands

ABSTRACT

An extension is presented to a time domain panel method for the seakeeping of high speed ships. The extension consists of the calculation of the free surface elevation by combining the solution of the potential problem with influence functions specially evaluated on a free surface grid. The free surface elevation together with the rigid body motions is used to correct the pressure distribution from the average submerged geometry to the actual submerged geometry. For this correction two methods are proposed: (1) correction of the hydrostatic pressure distribution and (2) stretching of the hydrodynamic pressure distribution.

Verifications are presented for the wave profile along a Wigley hull and a Series 60 hull, both traveling in calm water, showing reasonable similarity of calculations with experiments and a specialized nonlinear code. Validations are presented for the steady trim and rise of a slender and a non-slender high speed ship for a wide range of Froude numbers. Although trim and rise are still underpredicted, the stretching method improves the stability of the calculations greatly and is promising for unsteady seakeeping calculations.

KEY WORDS: Time-domain; seakeeping; high speed; diffraction; potential flow; free surface elevation; pressure stretching.

INTRODUCTION

Recently, large numbers of high speed craft have been constructed for applications ranging from naval operations, coast guard duties, and SAR operations to offshore supply and passenger transport. Although a significant dynamic lift is developed, these vessels are mostly not fully planing at their operational speeds, with typical Froude numbers ranging from 0.6 to 1.2. The high speed combined with rough weather conditions at open sea results in challenging design requirements. For instance, operability has to be ensured at operational conditions, for example by setting a maximum to the acceleration levels of the ship. Additionally, the structure of the vessel needs to cope with the loads encountered during its operation. Both requirements necessitate to have a practical seakeeping analysis tool, able to provide insight in the motions and loads developed in a seaway during the design process.

Different computational models have been developed for seakeeping of high speed craft. Two-dimensional added mass strip theory, developed by Von Karman (1929) and Wagner (1932) in the thirties, considers planing equivalent to the impact of two-dimensional wedges on a free surface. Zarnick (1978), Faltinsen & Zhao (1994), and Keuning (1994) (amongst others) have developed efficient semi-empirical computational models for planing craft in waves based on this theory. Tulin (1956) and Vorus (1996) (amongst others) applied two-dimensional potential theory on impacting wedges, providing a numerical solution to the two-dimensional problem.

Additionally, three-dimensional methods have been applied to high speed ships. Three-dimensional frequency domain boundary element methods have been applied for high speed hulls with transom sterns, for example by Ahmed et al. (2004). Another method under development for high speed ships is the vortex lattice method (3D VLM) developed by Lai & Troesch (1995) for planing ships, capable of steady high speed planing.

The current research is aimed at developing a practical tool for the evaluation of the seakeeping behavior of high speed vessels and to provide an input for structural strength analysis. A three-dimensional transient Green function method for large amplitude ship motions is chosen because of a number of advantages over the previously described methods:

- The transient free surface Green function enables the method to deal with significant forward speeds, as shown by for example King et al. (1988). 3D VLM and added mass striptheory were developed for fully planing and their applicability is limited for lower forward speeds. 3D diffraction theory is only valid for very low forward speeds, because of difficulties with the correct implementation of forward speed in the frequency-domain free surface Green function.
- The method is fully capable of dealing with unsteady three-dimensional (large amplitude) motions. The two-dimensional methods have problems dealing with typical three-dimensional flows occurring with asymmetrical motions. Nevertheless, effort has been undertaken to include these motions, for example by Xu et al. (1998). The applicability of 3D VLM to unsteady seakeeping problems is complicated as well, due the fact that the free surface boundary condition is only satisfied in a very limited region near the body. The limited application of the free surface boundary condition makes it difficult to correctly deal with free surface effects associated with waves.

The formulation of the numerical model is based on the work of Lin and Yue (1990) and further developed by Van Walree (2002, 1999) and Pinkster (1998). The formulation adopted by Van Walree combines unsteady impulsive sources on the hull with doublet-elements to represent

lifting control surfaces. The free surface boundary conditions are linearized to the undisturbed free surface, while it is possible to retain the body boundary condition on the actual submerged geometry. Practically, it is necessary to linearize the body boundary condition as well, to limit the computational burden of the method, enabling the seakeeping analysis to run on a normal desktop computer. The underlying method is capable of dealing with submerged lifting surfaces and the corresponding wake sheets by using doublet and vortex elements. Inclusion of these elements is possible and can be done in a straightforward way similar to the original method presented by Van Walree (2002), but is omitted here.

A modification is presented that includes a higher order correction in the pressure distribution due to the free surface elevation combined with the rigid body motions. The method involves the calculation of the free surface elevation, the submerged geometry, and the subsequent correction of the pressure distribution. This correction has been elaborated in two different schemes:

1. The correction of the pressure distribution by modifying the hydrostatic pressure distribution.
2. The correction of the pressure distribution by stretching of the hydrodynamic pressure distribution.

In both schemes effort has been taken to correctly include non-linear Froude-Krylov contributions due to the incoming waves. The correction of the pressure distribution provides a way to partially correct the implications of the linearization of the free surface boundary condition and linearization of the body geometry, improving the seakeeping predictions and the time-varying nature of the pressure distribution.

The second section will shortly describe the mathematical formulation of the problem and will detail the calculation of the free surface elevation, the submerged geometry, and the pressure corrections. In the third section, verification and validation results are presented for the free surface deformation, the steady trim and rise of high speed vessels, and the unsteady motions of a high speed craft in a seaway. The final section will summarize the conclusions and recommendations that follow from the research presented in this paper.

NUMERICAL FORMULATION

The numerical method presented in this paper is an extension of the work presented by Lin and Yue (1990), Pinkster (1998) and Van Walree (2002). In the first subsection a short description of the fundamentals of the method is given, followed by a more extensive mathematical formulation of the extension of the method for the calculation of the free surface deformation and the correction of the hydromechanic pressures.

Time domain Green function method

Potential flow is assumed based on the following simplifications of the fluid:

- The fluid is homogeneous.
- The fluid is incompressible.
- The fluid is without surface tension.
- The fluid is inviscid and irrotational.

The medium of interest is water, while there is an interface with air. The ambient pressure p_a is assumed to equal zero. The water depth is infinite and waves from arbitrary directions are present. Under all these assumptions it can be shown that the Laplace equation, resulting from conservation of mass, is valid in the interior of the fluid:

$$\nabla^2 \Phi = 0 \tag{1}$$

The fluid domain $V(t)$ is considered, bounded by the free surface of the fluid $S_F(t)$, the submerged part of the hull of the ship $S_H(t)$ and the surface bounding the fluid infinitely far from the body $S_\infty(t)$. Assuming linearity, the total potential Φ can be split into two parts:

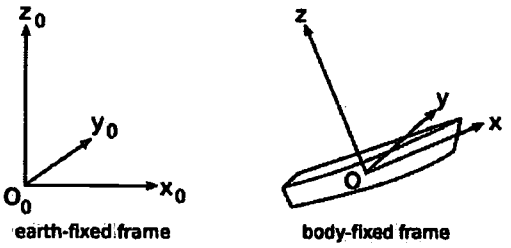

Fig. 1. Coordinate systems, x_0y_0-plane coincides with still water free surface

$$\Phi = \Phi^w + \Phi^d \tag{2}$$

Where Φ^w is the incident wave potential, Φ^d is representing the disturbance of the flow caused by the motions of the body and $-Ux$ represents the uniform incoming flow due the forward motion of the ship. The wave potential Φ^w is given by:

$$\Phi^w = \frac{\zeta_a g}{\omega} e^{kz} \sin\left(k\left(x_0 \cos\psi + y_0 \sin\psi\right) - \omega t\right) \tag{3}$$

The subscript '0' refers to earth fixed coordinates, as shown in Fig. 1. At the free surface two conditions are imposed. First, a kinematic condition assuring that the velocity of a particle at the free surface is equal to the velocity of the free surface itself.

$$\frac{\partial \eta}{\partial t} + \nabla\Phi \cdot \nabla\eta - \frac{\partial z_0}{\partial t} = 0 \quad \forall\, \mathbf{x_0} \in S_F \tag{4}$$

Where η is the vertical free surface displacement. Second, a dynamic condition assuring that the pressure at the free surface is equal to the ambient pressure. For this condition use is made of the unsteady Bernoulli equation in a translating coordinate system.

$$\frac{\partial \Phi}{\partial t} + g\eta + \frac{1}{2}\left(\nabla\Phi\right)^2 = 0 \quad \forall\, \mathbf{x_0} \in S_F \tag{5}$$

Both can be combined and linearized around the still water free surface, yielding:

$$\frac{\partial^2 \Phi}{\partial t^2} + g\frac{\partial z_0}{\partial t} = 0 \quad \text{at } z_0 = 0 \tag{6}$$

On the instantaneous body surface $S_H(t)$ a zero normal flow condition is imposed:

$$V_n = \frac{\partial \Phi^d}{\partial n} + \frac{\partial \Phi^w}{\partial n} \quad \forall\, \mathbf{x_0} \in S_H \tag{7}$$

where V_n is the instantaneous normal velocity of the body. For a large distance from the body (at infinity, S_∞) the influence of the disturbance has to vanish.

$$\Phi^d \to 0 \quad \frac{\partial \Phi^d}{\partial t} \to 0 \tag{8}$$

At the start of the process, apart from the incoming waves, the fluid is at rest, as is reflected in the initial condition.

$$\Phi^d\Big|_{t=0} = \frac{\partial \Phi^d}{\partial t}\Big|_{t=0} = 0 \tag{9}$$

In this time-domain potential code the Green function given in Eq. 10 will be used. This Green function specifies the influence of a singularity with impulsive strength (submerged source or doublet) located at singularity point $q\,(\xi,\eta,\zeta)$ on the potential at field point $p\,(x_0,y_0,z_0)$.

$$G\,(p,t,q,\tau) = G^0 + G^f = \frac{1}{R} - \frac{1}{R_0} + 2\int_0^\infty \left[1 - \cos\left(\sqrt{gk}\,(t-\tau)\right)\right] e^{k(z_0+\zeta)} J_0\,(kr)\,dk \quad \text{for } p \neq q\,,\, t \geq \tau \qquad (10)$$

In Eq. 10 G^0 is the source and doublet plus biplane image part (or Rankine part), while G^f is the free surface memory part of the Green's function. J_0 is the Bessel function of order zero.
It has been shown, by for example Pinkster (1998), that the function G satisfies both the Laplace equation and the boundary conditions, making it a valid solution for the boundary value problem stated above.

Using the above, it is possible to derive a boundary integral formulation. In this derivation first Green's second identity is applied to $\Phi^d\,(\mathbf{x}_0,t)$ and $\frac{\partial G}{\partial \tau}\,(\mathbf{x}_0,\boldsymbol{\xi},t-\tau)$. Next, the free surface integral is eliminated by virtue of the Green function. Finally, a general formulation of the nonlinear integral equation is obtained for any field point p:

$$4\pi T\Phi^d\,(p,t) = -\int_{S_{HLW}(t)} \left(\Phi^d G_n^0 - G^0\Phi_n^d\right) dS + \int_0^t d\tau \int_{S_{HLW}(\tau)} \left(\Phi^d G_{\tau n} - G_\tau \Phi_n^d\right) dS + \frac{1}{g}\int_0^t d\tau \int_{C(\tau)} \left(\Phi^d G_{\tau\tau} - G_\tau \Phi_\tau^d\right) \mathbf{V}_n^{(2D)} dL \qquad (11)$$

Where for example $G_n^0 = \partial G^0/\partial n$ and T is defined as:

$$T\,(p) = \begin{cases} 1 & p \in V\,(t) \\ 1/2 & p \in S_H\,(t) \\ 0 & \text{otherwise} \end{cases} \qquad (12)$$

A source distribution σ will be distributed on the body surface S_H. The source strength is set equal to the jump in the normal derivative of the potential between the inner (-) and outer (+) sides of the body surface. As no doublet distribution is present on S_H, the jump in potential across S_H is set to zero.

$$\left.\begin{array}{l} \Phi^{d+} - \Phi^{d-} = 0 \\ \dfrac{\partial \Phi^{d+}}{\partial n} - \dfrac{\partial \Phi^{d-}}{\partial n} = \sigma \end{array}\right\} \forall \quad q \in S_H \qquad (13)$$

Note that T =1/2, because p lies on the boundary, thus using Eq. 13 yields:

$$4\pi\left(V_{n_p} - \frac{\partial \Phi^w}{\partial n_p}\right) = 2\pi\sigma_p + \oint_{S_H(t)} \sigma\,(q,t)\,\frac{\partial G^0}{\partial n_p} dS - \int_0^t d\tau \int_{S_H(\tau)} \sigma\,(q,\tau)\,\frac{\partial^2 G^f}{\partial t \partial n_p} dS + \frac{1}{g}\int_0^t d\tau \int_{L_W(\tau)} \sigma\,(q,\tau)\,\frac{\partial^2 G^f}{\partial t \partial n_p} V_N V_n dL \qquad (14)$$

In this equation $\partial/\partial n_p$ indicates a normal derivative at the field point p $\partial/\partial n_q$ at singularity point q. Eq. 14 is the principal equation to be solved for the unknown source strengths $\sigma\,(q,t)$. The equation is discretized in terms of a source element distribution on S_H. In the current method constant strength quadrilateral source panels are used.

At the start, $t = 0$, the body is impulsively set into motion. At each subsequent time step the body is advanced to a new position with an instantaneous velocity. Both position and velocity are known from the equations of motion. The discretized form of Eq. 14 is solved to obtain the source strengths at each time step.

Especially the evaluation of the free surface memory term of the Green's function G^f requires a large amount of computational time. These terms need to be evaluated for each control point for the entire time history at each time step. To decrease this computational burden, the evaluation of G^f has been simplified. For low $(t-\tau)$ values use is made of interpolation of predetermined values for G^f, while for larger $(t-\tau)$ values polynomials and asymptotic expansion are used to approximate G^f.

Moreover, the position of the hull and lifting surfaces relative to the past time panels is not constant due to the unsteady motions, making recalculation of the influence of past time panels necessary for the entire time history. This recalculation results in a computational burden requiring the use of a supercomputer. To avoid this burden, the unsteady position of hull and lifting surfaces is linearized to the average position (moving with the constant forward speed). Now the memory integral can be calculated a priori for use at each time step during the simulation.

Forces can be obtained from integration of the pressure at each collocation point over the body. The pressures can be obtained by using the unsteady Bernoulli equation (in a body fixed axis system):

$$\frac{p_a - p}{\rho} = \frac{1}{2}\left\{\left(\frac{\partial \Phi}{\partial x}\right)^2 + \left(\frac{\partial \Phi}{\partial y}\right)^2 + \left(\frac{\partial \Phi}{\partial z}\right)^2\right\} + \frac{\partial \Phi}{\partial t} - \mathbf{V}\cdot\nabla\Phi \qquad (15)$$

Where $\mathbf{V}$ is the total velocity vector at the collocation point of the rigid body, including rotations.

The only difficulty remaining is to obtain the time derivative of the potential for the source panels, as a straightforward backward difference scheme gives unstable results. This instability is solved by a more accurate scheme, detailed by Van Walree (2002).

Free surface evaluation

Free surface elevation. The free surface elevation can be derived from the free surface boundary condition given in Eq. 6. The linearized dynamic condition (Eq. 5) can be used to obtain an expression for the free surface elevation:

$$\eta = -\frac{1}{g}\frac{\partial \Phi}{\partial t} \quad \text{at } z_0 = 0 \qquad (16)$$

$\frac{\partial}{\partial t}$ is the time derivative for an earth-fixed (inertial) coordinate frame. The free surface elevation is to be known in a ship-fixed system, making a transformation necessary. Now, the free surface elevation in the body-fixed system becomes:

$$\eta = -\frac{1}{g}\frac{\partial \Phi}{\partial t} + \frac{1}{g}\left[\mathbf{V_O} + \boldsymbol{\Omega} \times \mathbf{r}\right]\cdot\nabla\Phi \qquad (17)$$

The vector $\mathbf{V_O}$ is the velocity of the origin of the ship-fixed coordinate system, resolved into the instantaneous x,y,z directions of this frame, $\boldsymbol{\Omega} = (p,q,r)$ is the rate of rotation of the body's frame of reference and $\mathbf{r} = (x,y,z)$ is the position vector.

For an unsteady problem, where the body boundary condition is linearized to the mean position of the body the free surface elevation can be calculated by setting $\mathbf{V} = [U_{vel}\ 0\ 0]$, where U_{vel} is the steady forward speed.

$$\eta = -\frac{1}{g}\frac{\partial \Phi}{\partial t} + \frac{U_{vel}}{g}\frac{\partial \Phi}{\partial x} \qquad (18)$$

Evaluation of the Green function contributions at the free surface. In order to calculate the free surface elevation, both the spatial derivatives and the time derivative of the velocity potential are needed at the free surface. To evaluate the spatial derivatives (the flow velocities U, V, W) Eq. 11 needs to be re-evaluated to obtain expressions for these derivatives at the free surface.

Again field point p is located on a boundary of the fluid domain, in this case the undisturbed free surface, thus $T = 1/2$ is set according to Eq. 12. The result is again yields Eq. 20, but now p is on the free surface instead of the body surface.

The U, V, W-components of V_p can be simply obtained by using the normal vector at the field point p at the free surface. Thus to obtain the flow velocities at the free surface it is sufficient to know the singularity strength σ of the body panels together with the Green function derivatives evaluated for the field point or field point distribution on the free surface. These Green function derivatives are only dependent on spatial coordinates and can be evaluated in the same way as for the main solution of the potential problem. The time derivative of the undisturbed wave potential can be calculated analytically, the time derivative of the source potential again cannot be calculated straightforwardly and the alternative approach is used again.

Free surface grid. A free surface grid is defined to calculate the intersection of the body in its actual position with the deformed free surface. The extend of the grid is slightly larger than the vertical projection of the ship to allow for the ship motions.

Additionally, it is possible that the instantaneous waterline intersection contour lies within the still water contour, for instance when the ship is displaced upwards. The potential problem however, is not mathematically defined for the free surface part inside the still water intersection contour. And although smooth, the resulting free surface elevation inside the body is in many cases extremely deformed; without any physical meaning. To avoid complications the following has been done:

- The free surface elevation due to incoming waves is separated from the free surface elevation due to the disturbance potential.
- The free surface elevation due to the disturbance is calculated on a grid consisting of transverse lines of grid points as shown in Fig. 2. The free surface elevation is only calculated on the external gridpoints. The elevation at the internal grid points is related to the elevation at the closest external grid points by linear interpolation, yielding the wave elevation for the internal grid points. The grid is shown in right hand side of Fig. 3.

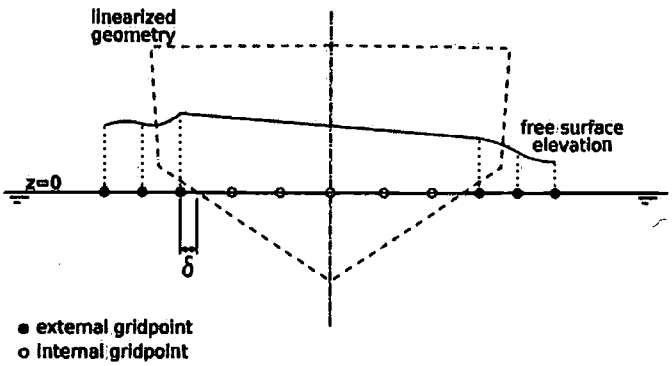

Fig. 2. Transverse free surface grid line

In order to obtain the intersection of the body with the free surface, information of the free surface elevation is needed at the panel locations of the body. To obtain this information, use is made of two-dimensional spline interpolation for the free surface elevation due to disturbance potential. The free surface elevation due to the incoming waves is directly calculated with the formulation of the incoming wave potential. The free surface elevation in all collocation points is shown in the left hand side of Fig. 3.

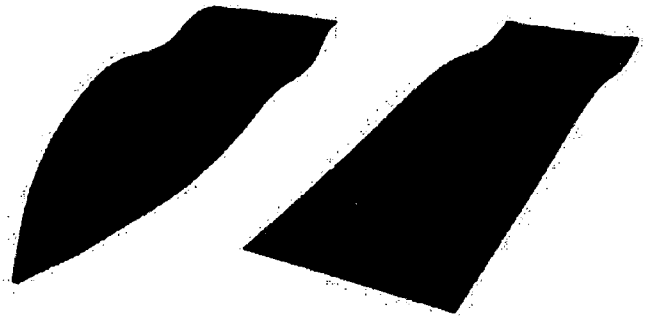

Fig. 3. Free surface elevation evaluation grid (right) and spline interpolation (left)

Correction of the pressure distribution

Due to the geometric linearization of the problem, the hydrodynamic pressure due to the disturbance potential is calculated at the still water wetted part of the body at all time instances. The variation of the wetted surface caused by the incoming waves, the diffracted and radiated waves, and the rigid body motions is ignored. Nevertheless, the pressure distribution can be corrected by considering the real earth-fixed position of each collocation point relative to the free surface obtained with the method described in the previous sections. This subsection details two possibilities for this pressure correction.

Method 1 Nonlinear correction of the hydrostatic pressures. The correction is elaborated for each pressure component. The still water free surface is $z_0 = 0$ and the actual free surface is $z_0 = \eta$; ζ is the incident wave elevation.

- Hydrostatic pressure p_s: The actual earth-fixed rigid body position is used for the calculation of the pressure.

$$\begin{aligned} p_s &= -\rho g z_0 && \forall \quad z_0 \leq 0 \wedge z_0 \leq \eta \\ p_s &= -\rho g\,(z_0 - \eta) && \forall \quad z_0 > 0 \wedge z_0 \leq \eta \\ p_s &= 0 && \forall \quad z_0 > \eta \end{aligned} \tag{19}$$

- Hydrodynamic pressure p_d: The hydrodynamic pressure, working on the still water submerged geometry, will be left unmodified, even when the originally submerged geometry emerges. Experience shows that when the hydrodynamic pressure is changed only by setting it to zero in emerged regions, the force balance becomes unstable.
- Froude-Krylov pressure p_w: The undisturbed wave pressure can be included by either by simply calculating the linear Froude-Krylov pressures directly at the undisturbed submerged geometry or by calculating the Froude-Krylov pressures at the actual submerged geometry. In the following the linear Froude-Krylov contribution is included on the actual position of the geometry up to the still water free surface.

  When the original 'dry' part becomes submerged due to rigid body motions combined with the free surface elevation the hydrostatic pressure changes into: $p_s = -\rho g\,(z_0 - (\eta - \zeta))$ to avoid taking into account the wave pressure twice (in the hydrostatic part and in the Froude-Krylov part).

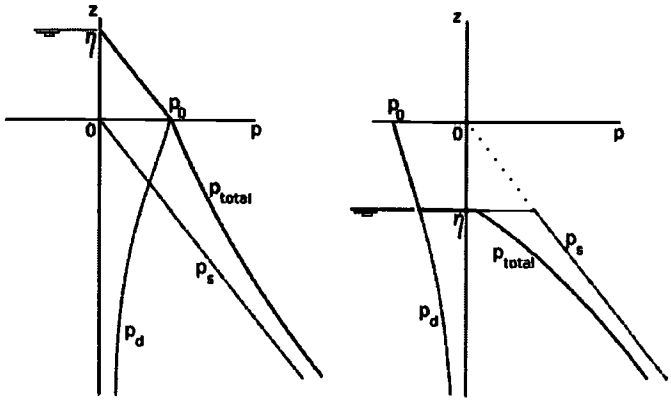

Fig. 4. Vertical pressure distribution for nonlinear hydrostatics, wave crest - left, wave trough - right

Fig. 4 shows how the modification of the hydrostatic pressure (dashed line marked p_s) impacts the total vertical pressure distribution (thick line marked p_{total}). Generally, wave crests do not pose problems. The pressure above the still water free surface is assumed to be hydrostatic and the hydrostatic pressure in the wave crest at the still waterline and the hydrodynamic pressure of the wetted surface at the waterline equal each other and no jump is present. In a wave trough however, a jump in pressure is occurring at the instantaneous free surface. One reason for this jump is the fact that the hydrodynamic pressure p_d is not set to zero in the wave trough above the free surface (to avoid instabilities in the force balance, as outlined above). Yet, setting the hydrodynamic pressure in a wave trough to zero still results in a pressure jump. This jump is due to the linearization of the free surface boundary condition.

A further complication is the inclusion of the rigid body motions (not shown in Fig. 4). Although the rigid body motions can be implemented easily by substituting the actual z_0-coordinate when calculating the hydrostatics, even more jumps will occur in the total pressure distribution.

A similar approach has been used by Blandeau et al. (1999) for a local pressure model on the side shell of FPSOs. They use the hydrodynamic pressures at the waterline in a zero forward speed frequency domain panel method. The pressure at the waterline is corrected by applying a watercolumn of height $\eta = p_0/\rho g$ in case of a wave crest and the pressure above a through is set to zero.

Although, this basically yields the same results in a wave crest and more computational efficient (no influence function evaluations on the free surface are needed), the use of waterline pressures has disadvantages for rapidly varying submerged geometries. This is especially true for high speed craft, with their V-shaped frames in the bow region and very shallow frames aft. Using the still waterline pressures then leads to very large inaccuracies.

Method 2 Non linear correction of the hydrodynamic pressures, As pointed out in the previous section, the inclusion of nonlinear corrections in the hydrostatic pressures yields inconsistencies resulting in jumps in the pressure distribution. These jumps are caused by retaining the hydrodynamic pressures, while adapting the hydrostatic pressures. For slow speed ships operating in non-steep waves generally this will not result in large deviations in the pressure distributions, as the disturbance part of the hydrodynamic pressure is relatively small in comparison with the hydrostatic and Froude-Krylov pressures.

Problems arise when the hydrodynamic disturbance pressures are relatively large. This is the case for high speed ships, where the high rate of change of impulse of the water along the length of the ship, especially at the bow, causes high hydrodynamic pressure regions. The resulting loads cause significant lift and thereby significant trim and rise. Variations in the hydrodynamic pressures will have significant effect on the total force balance of the ship. Especially for ships with relatively large length over beam ratios and flared bow sections, large variations in submerged geometry and thus in hydrodynamic loads can occur.

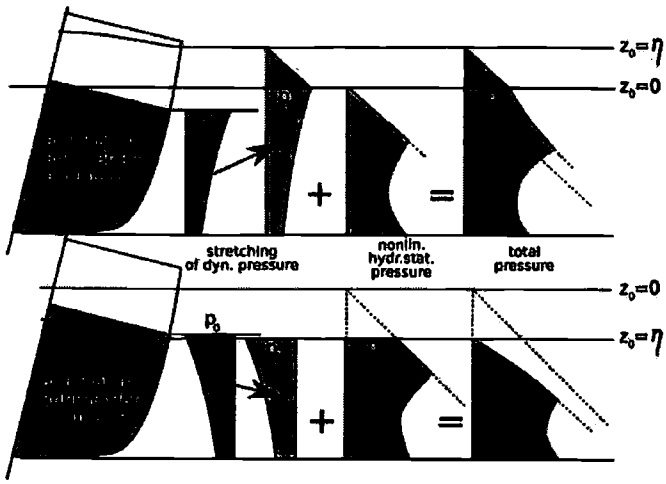

Fig. 5. Stretching of pressure for free surface elevation (top) and free surface depression (bottom)

Now a method is developed that consideres the influence of body and free surface nonlinearities (causing changes in the wetted surface) in the hydrodynamic loads as well. Hydrostatic pressures and hydrodynamic pressures are considered separately. The hydrodynamic pressures consist of disturbance and incident wave pressures.

- Hydrostatic pressure p_s: The actual earth-fixed rigid body position is again used for the calculation of the pressure.

$$\begin{aligned} p_s &= -\rho g z_0 \qquad \forall \quad z_0 \leq 0 \wedge z_0 \leq \eta \\ p_s &= 0 \qquad\qquad\ \forall \quad z_0 > 0 \wedge z_o > \eta \end{aligned} \tag{20}$$

- Hydrodynamic pressure $p_d + p_w$: for the treatment of the hydrodynamic pressures two different cases need to be considered:

  (1) Free surface elevation (wave crest - Fig. 5, top). The hydrodynamic pressures are stretched vertically from the original wetted depth (keel to still water line in rest) to the actual earth-fixed wetted depth, measured from the earth-fixed position of the keel to the earth-fixed still water surface. For the part of the hull in between the earth-fixed still water surface and the actual free surface elevation a hydrostatic pressure distribution is assumed. This process eliminates jumps, because at the $z_0 = 0$ surface the hydrostatic pressure of the wave crest $\rho g\,(\eta - z_0) \ \wedge \ z_0 = 0$ is equal to the hydrodynamic pressure at the waterline p_0, as can be seen be comparing Eq. 18 with Eq. 15 evaluated at $z = 0$ (ignoring the $\nabla\Phi \cdot \nabla\Phi$ term at $z = 0$). Additionally, the zero-pressure condition at the water-air interface is satisfied.

  (2) Free surface depression (wave trough - Fig. 5, bottom). The hydrodynamic pressures are stretched vertically from the original wetted depth (keel to still water line in rest) to the actual wetted depth (including changes in wetted depth due to the rigid body motions and free surface deformations). Again pressure jumps are eliminated and the pressure at the water-air interface is again zero. The hydrostatic pressure is at the interface equal to $\rho g\eta$, while the hydrodynamic pressure at the interface $p_0 = -\rho g\eta$, again this can be shown by evaluating Eq. 15 at $z = 0$ (ignoring the $\nabla\Phi \cdot \nabla\Phi$ term at $z = 0$), together with Eq. 18.

The Froude-Krylov pressures and the hydrodynamic disturbance pressures are both evaluated at the still water wetted surface, before they

are stretched to the actual wetted surface. It is possible in this process to evaluated the Froude-Krylov pressures by using the actual earth-fixed coordinates, instead of the linearized still water wetted surface coordinates.

Incorporation in the potential solver. Both methods are simply incorporated in the time domain scheme by modifying the pressures obtained from the solution of the potential flow at each time step. The modified pressures are used to solve the equation of motion in a Runge-Kutta loop. Next the geometry is displaced forward with the constant forward speed times the time step and the next step is commenced.

VERIFICATIONS AND VALIDATIONS

Verification of the stationary component of the free surface elevation

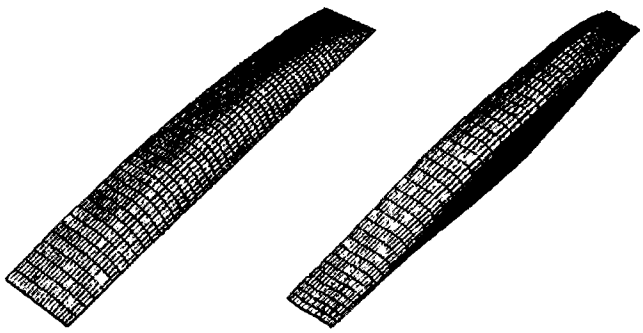

Fig. 6. Panel arrangement on Wigley hull (left) and Series 60 $C_b = 0.60$ (right)

To verify the scheme, calculations were performed on a Wigley hull and a Series 60 $C_b = 0.60$ in calm water to obtain the steady wave profile. The Wigley had a length over beam ratio of 10, a length beam over draught ratio of 1.6, and 1000 panels. The Series 60 had a length over beam ratio of 7.3, a length beam over draught ratio of 2.5, and 1128 panels. We calculated the wave elevation with the numerical code presented in this paper and compared it to results of experiments and of a nonlinear raised panel method with free surface discretization, published by Raven (1996). The comparisons solely served as a verification of the calculated free surface elevation. The code under development is not meant as a tool to predict the steady wave system and wave resistance. The panel arrangement of both hulls is depicted in Fig. 6.

The wave profile for the Wigley at $Fn = 0.316$ with zero trim and rise is presented in Fig. 7. Although the linearized Green function performs slightly worse than the raised panel code, still the results are fairly accurate. The position of bow wave and following troughs and crests were calculated in the right position. The bow wave height was slightly underestimated; along the hull the solution oscillated slightly around the Rapid solution and the measurements.

In Fig. 8 the wave profile is depicted for the Series 60 $Cb = 0.60$ hull at $Fn = 0.316$ with zero trim and rise. For this more shiplike hull the bow wave lagged a little behind the experiments and the Rapid calculations. The position of the other crests and troughs was more accurate. Still, crests and troughs were underestimated.

In conclusion, it showed that the linearized code clearly performs less than the raised panel code for the estimation of the steady hull wave profile. Although the position of crests and troughs was estimated accurate enough, the code underestimated their height, this can be attributed to the free surface linearization. Nevertheless, the main purpose of including the free surface elevation into the calculations was the influence on the seakeeping behavior and not the stationary wave generation itself.

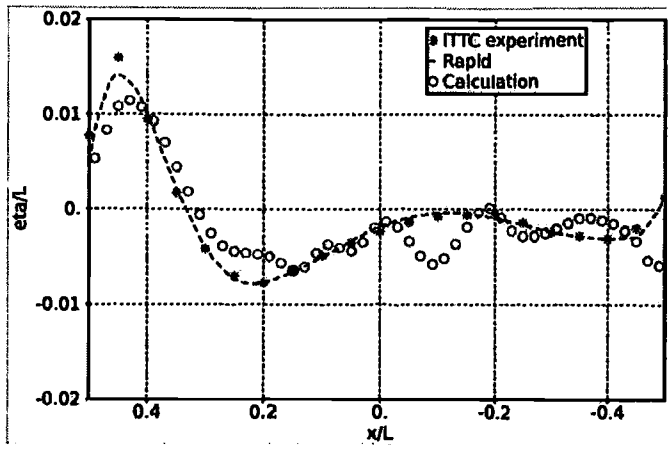

Fig. 7. Wave profile along a Wigley hull at $Fn = 0.316$, calculations compared with raised panel method calculations and ITTC experiments

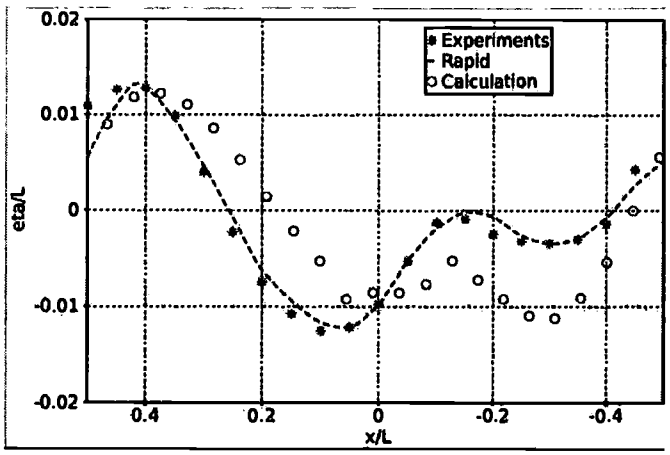

Fig. 8. Wave profile along a Series 60 hull at $Fn = 0.316$ with $C_b = 0.60$, calculations compared with raised panel mathod calculations and experiments

Trim and rise for two high speed ships

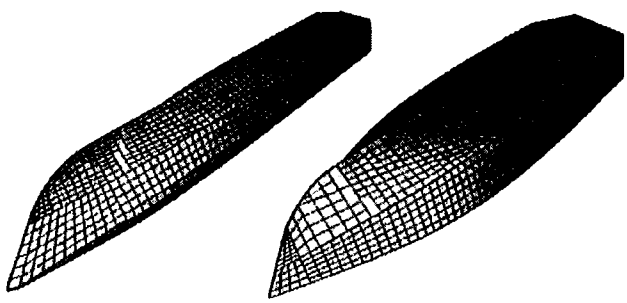

Fig. 9. Panel arrangement on ESC (left) and on D19 (right)

Before seakeeping calculations could be performed the submerged body paneling had to be determined. This is dependent on the trim and rise

at the forward velocity under consideration. A series of calculations was performed to find the trim and rise, and thus the submerged geometry. iteratively. The start and end positions of each calculation, consisting of a run at constant forward speed in calm water, were compared. When the difference was less than a predetermined convergence criterion, the submerged paneling and the reference position converged. The steady trim and rise were now known for that speed. Typical convergence criterions were 0.02 m full scale difference between start and end of a calculation for the rise and 0.1 deg for the trim. To improve on the stability of the iterative procedure we implemented a bisection method, using average of the last two calculations as input for the current.

We performed the steady trim and rise calculations on two high speed ships, designated ESC and D19. The ESC, or 'Enlarged Ship Concept' was a slender monohull of 55 m length and a length over beam ratio of 6.5. The hull has 25 deg deadrise amidships with both aftbody twist and an inclined centerline aft. A more detailed description is given by Keuning & Van Walree (2006). The D19 was a non-slender monohull with $L/B = 3.6$. The hull had 19 deg deadrise with a prismatic aftbody. In Fig. 9 the panel arrangements of both models is depicted. Both models typically had 1200 panels on the submerged part, enough for ensuring a grid independent solution.

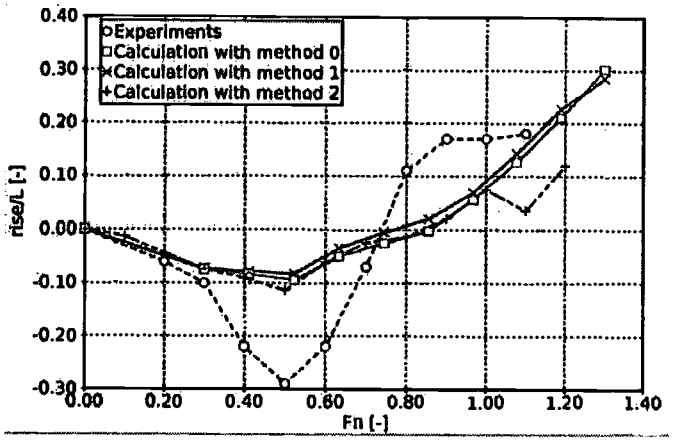

Fig. 10. Steady rise of slender fast monohull ESC (rise negative: sinkage)

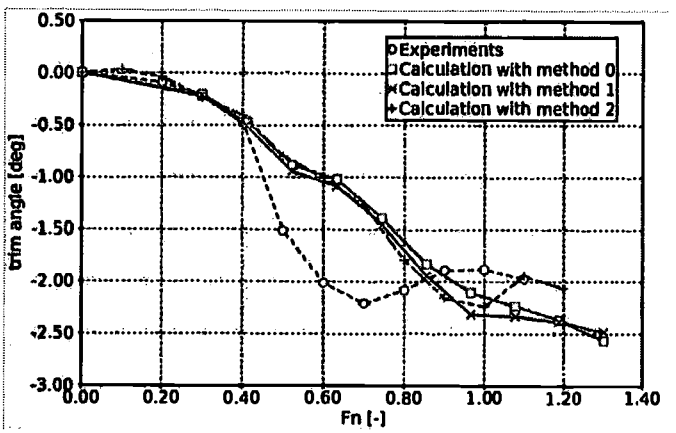

Fig. 11. Steady trim of slender fast monohull ESC (trim positive: bow down)

Figs. 10 and 11 show the rise and trim against the Froude number of the ESC. Three different calculation schemes, using different pressure modifications, were compared with the result of model experiments performed in the large basin of the Ship Hydromechanics Laboratory of Delft University of Technology. Calculations marked '0' are the results of the original version of the code without pressure modifications, calculations marked '1' are results with the first pressure modification (hydrostatics), and calculations marked '2' are results with the second pressure modification (stretched hydrodynamics, nonlinear hydrostatics). Figs. 12 and 13 show the same results for the D19 hull. although results of the original version of the code are omitted here.

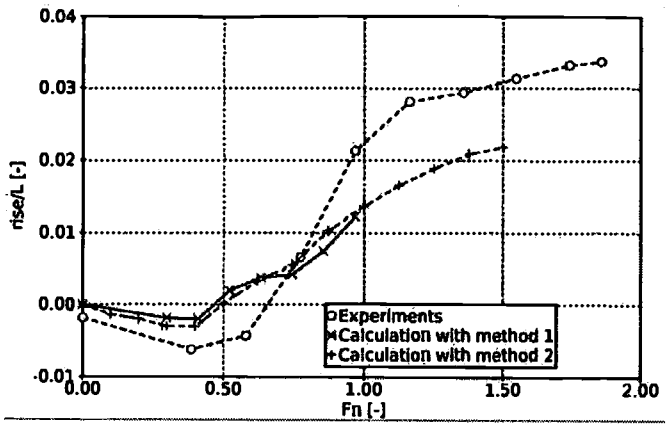

Fig. 12. Steady rise of non-slender fast monohull D19

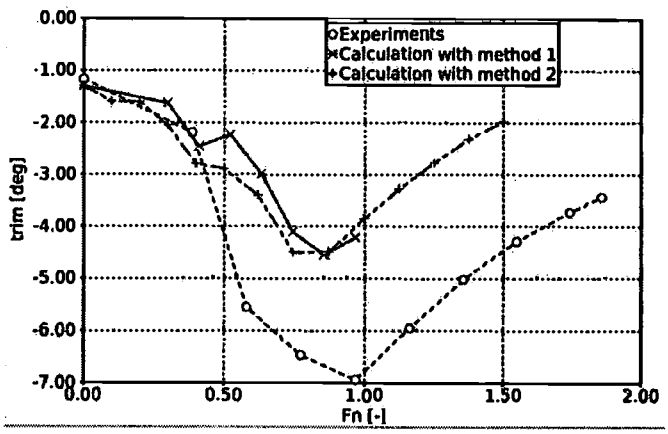

Fig. 13. Steady trim of non-slender fast monohull D19

As the pressure modifications dealt with two issues, (1) the geometric nonlinearities due to rigid body motions and (2) the free surface nonlinearities due to wave making, it was expected to see the effect of both in two different ways. On the one hand, the iterative scheme was made to match the steady submerged geometry and the numerical paneling, effectively removing geometric nonlinearities. In other words the geometric effects were not expected to show up in the calculated trim and rise. On the other hand, it was expected that the steady wave system would cause an additional trimming moment, especially at high speeds. The modified version of the code possibly would correct for this.

For the ESC it was evident that both pressure modifications hardly influenced the steady trim and rise. The second pressure modification, stretching, resulted in slight deviations in both trim and rise at speeds above $Fn = 1.0$. Clearly, the steady wave system hardly influenced the lift and the trimming moment, what can be attributed to the very slender bow shape of the ESC. Moreover, the slender bow shape with high deadrise limited the geometric variations of the submerged body

strongly. The hull behaved very 'linear', making pressure corrections unnecessary.

The steady trim and rise of the D19 were hardly influenced as well by the pressure modification method used. Nevertheless, the wide body with relatively small deadrise suffered from large geometric variations. Especially for high speeds above $Fn = 0.60$ these variations could not be balanced by modification of the hydrostatics alone and method 1 failed to yield convergence above Froude number 0.9. Method 2 however, was able to stabilize the geometric variations by stretching of the hydrodynamic pressure distribution and gave results up to Froude numbers of 1.5 and higher. The stability and convergence of the iterative procedure were strongly improved by the second method. This indicates a possible beneficial effect of the hydrodynamic pressure stretching method on unsteady seakeeping calculations by better capturing the pressure variations.

Both validations showed a lack of suction (sinkage) at low speeds and a lack of rise and trim at high speeds. This indicated that the hydrodynamic lift was underestimated by the current setting of the potential problem. As only a source distribution is used, no circulation lift was possible. Nevertheless, it is possible to add circulation lift within the framework of the code by using doublet elements and corresponding wake sheets. This will be researched in the near future.

CONCLUSION

An extension to a linearized time domain panel method was presented for the analysis of the seakeeping of high speed ships. The extension consisted of a correction on the pressure distribution to account for geometric nonlinearities due to rigid body motions and free surface nonlinearities due to the free surface deformation. Two pressure modification methods were proposed:

1. Modification of the hydrostatic pressures to account for rigid body motions and free surface elevation.
2. Modification of the hydrodynamic pressures using a stretching method that takes into account the rigid body motions and the free surface elevations.

Both methods necessitated the evaluation of the free surface elevation due to radiation, diffraction, and incident waves on a special free surface grid.

Verifications of the free surface profile along a Wigley and a Series 60 hull showed that the code is able to predict the steady free surface elevation reasonably well for the purposes of the method. Off course, specialized nonlinear methods with free surface paneling perform better, but either lack the capability of dealing with unsteady seakeeping or are very computatively expensive.

Next, the results of steady trim and rise calculations were shown for two high speeds ships, one slender and one non-slender. The pressure modification did not have a significant influence on the resulting trim and rise, yet the second, stretching, method improved the convergence of trim and rise calculations dramatically, especially for the small L/B hull and at high forward speed. One the one hand, this means that the stretching method dealt adequately with the large variations occurring in the hydrodynamic pressure distribution due to the large submerged geometry variations. On the other hand, this means that the steady wave system generated by both hulls, hardly influences the trim and rise of both designs. Additionally, it can be concluded that the slender hull suffered less from the geometric variations and seemed to perform much more 'linear'.

Both validation cases showed a significant lack of sinkage at low speeds and trim and rise at high speeds. Most probably this lack is caused by a absence of circulation lift in the model due to the use of source panels. It is expected that the inclusion of circulation lift in the numerical model could improve the predictions significantly. Therefore, future work includes the adaptation of the model for use of doublet elements on the hull together with a wake sheet.

ACKNOWLEDGEMENTS

The authors gratefully acknowledge the permission of the participants of the FAST project: Royal Netherlands Navy, Damen Shipyards at Gorinchem (NL), Royal Schelde Group at Vlissingen (NL), United States Coast Guard at Baltimore (USA), Marin at Wageningen (NL), and the TUDelft (NL) to use the experimental results of the FAST project.

REFERENCES

Ahmed, T. M., D. A. Hudson, and P. Temarel (2004). Incorporation of steady flow effects in linear three-dimensional seakeeping predictions for high speed hulls. In *Proceedings of the Ninth Symposium on Practical Design of Ships and Other Floating Structures*, pp. pp. 496–503.

Blandeau, F., M. Francois, S. Malenica, and X. Chen (1999). Linear and non-linear wave loads on FPSOs. In *Proceedings of the Ninth International Offshore and Polar Engineering Conference*, Brest, France.

Faltinsen, O. and R. Zhao (1994). Numerical predictions of ship motions at high forward speed. *Phil. Trans. R. Soc.*, pp. 241–252.

Keuning, J. A. (1994). *The nonlinear behaviour of fast monohulls in head waves*. PhD dissertation, Delft University of Technology, Shiphydromechanic Laboratory.

Keuning, J. A. and F. Van Walree (2006). The comparison of the hydrodynamic behaviour of three fast patrol boats with special hull geometries. In *Fifth International Conference on High Performance Marine Vehicles*, pp. pp. 137–152.

King, B. K., R. F. Beck, and A. R. Magee (1988). Seakeeping calculations with forward speed using time-domain analysis. In *Proceedings 17th Symposium on Naval Hydrodynamics*, pp. pp. 577–596.

Lai, C. and A. W. Troesch (1995, March). Modeling issues related to the hydrodynamics of three-dimensional steady planing. *Journal of Ship Research 39*(1), pp. 1–24.

Lin, W. M. and D. Yue (1990). Numerical solutions for large-amplitude ship motions in the time domain. In *Proceedings of the 18th symposium on naval hydromechanics*, Ann Arbor, pp. pp. 41–65.

Pinkster, H. J. M. (1998). Three dimensional time-domain analysis of fin stabilised ships in waves. Master's thesis, Delft University of Technology, Department of Applied Mathematics.

Raven, H. C. (1996). *A solution method for the nonlinear ship wave resistance problem*. PhD dissertation, Delft University of Technology.

Tulin, M. P. (1956). The theory of slender surfaces planing at high speeds. *Schiffstechnik 4*, pp. 125–133.

Van Walree, F. (1999). *Computational methods for hydrofoil craft in steady and unsteady flow*. Ph. D. thesis, Delft University of Technology.

Van Walree, F. (2002, July). Development, validation and application of a time domain seakeeping method for high speed craft with a ride control system. In *Proceedings of the 24th symposium on naval hydrodynamics*.

Von Karman, W. (1929). The impact of seaplane floats during landing. Technical Memorendum TN 321, NACA.

Vorus, W. S. (1996, June). A flat cylinder theory for vessel impact and steady planing resistance. *Journal of Ship Research 40*(2), pp. 86–106.

Wagner, H. (1932). Uber Stoss und Gleitvorgange an der Oberfläche von Flüssigkeiten. *Zeitschrifft für Angewandete Mathematik und Mechanik 12*(4).

Xu, L., A. W. Troesch, and W. S. Vorus (1998, Sept.). Asymmetric vessel impact and planing hydrodynamics. *Journal of Ship Research 42*(3), pp. 187–198.

Zarnick, E. E. (1978, March). A nonlinear mathematical model of motions of planing boats in regular head waves. Report 78-032, DTNSRDC.